How to cite: *Angew. Chem. Int. Ed.* **2024**, *63*, e202405123
doi.org/10.1002/anie.202405123

Charge Transfer

Ultrafast Formation of Charge Transfer Trions at Molecular-Functionalized 2D MoS_2 Interfaces

*Yuancheng Jing, Kangkai Liang, Nicole S. Muir, Hao Zhou, Zhehao Li, Joseph M. Palasz, Jonathan Sorbie, Chenglai Wang, Scott K Cushing, Clifford P. Kubiak, Zdeněk Sofer, Shaowei Li, and Wei Xiong**

Abstract: In this work, we investigate trion dynamics occurring at the heterojunction between organometallic molecules and a monolayer transition metal dichalcogenide (TMD) with transient electronic sum frequency generation (tr-ESFG) spectroscopy. By pumping at 2.4 eV with laser pulses, we have observed an ultrafast hole transfer, succeeded by the emergence of charge-transfer trions. This observation is facilitated by the cancellation of ground state bleach and stimulated emission signals due to their opposite phases, making tr-ESFG especially sensitive to the trion formation dynamics. The presence of charge-transfer trion at molecular functionalized TMD monolayers suggests the potential for engineering the local electronic structures and dynamics of specific locations on TMDs and offers a potential for transferring unique electronic attributes of TMD to the molecular layers.

[*] Y. Jing, N. S. Muir, J. M. Palasz, J. Sorbie, C. Wang, C. P. Kubiak, S. Li, W. Xiong
Department of Chemistry and Biochemistry
University of California, San Diego
9500 Gilman Drive, MC 0358, La Jolla, California 92093-0358, United States
E-mail: w2xiong@ucsd.edu

K. Liang, H. Zhou, Z. Li, S. Li, W. Xiong
Material Science and Engineering Program
University of California, San Diego
9500 Gilman Drive, MC 0418, La Jolla, California 92093-0418, United States

S. K Cushing
Division of Chemistry and Chemical Engineering
California Institute of Technology
1200 E California Blvd, MC 127–72, Pasadena, California 91125, United States

Z. Sofer
Department of Inorganic Chemistry
University of Chemistry and Technology, Prague
Technická 5, 166 28 Prague 6, Czech Republic

Introduction

Transition metal dichalcogenides (TMDs) are a group of materials that are composed of a transition metal atom M from Group III or IV covalently connecting to two chalcogen atoms X in a hexagonal lattice.[1] The layered structure exhibits weak interlayer van der Walls interactions, which reduces the electrostatic screening and thereby gives rise to novel many-body interactions between charge carriers.[2] At the monolayer limit, the reduced dimensionality, combined with the reduction of screening for Coulomb interactions, leads to the emergence of various robust quasiparticles even at room temperature. These includes excitons,[3] trions[4] and bi-exciton,[5] several of which are unattainable in other systems.[6,7] Trions, for instance, are one such charged excitons, i.e. one exciton bounded with an additional charge carrier. They arise from the interaction between excitons and residual free charge carriers in monolayer TMDs.[4,6,7] The existence of trions allows electrically guiding and controlling charged particles more efficiently than excitons.[8,9]

To harness the unique characteristics of monolayer TMD due to many-body interactions, it is essential to finely adjust the materials' electro-optical properties and to transfer these distinct traits to other materials. One efficient approach is to create heterojunctions, including TMD-TMD[10–12] and molecule-TMD heterojunctions.[13–17] For example, it was recently shown that many-body control of electron localization in moiré heterostructures can greatly improve catalytic performance.[18] Similarly, doping monolayer TMD with molecules could control interfacial band alignment and its chemical and electrostatic environments.[19] In the meantime, due to the relatively weak screening along the normal direction of the interfaces, the heterojunction may potentially inherit the electronic properties of monolayer TMDs. For example, the existence of interfacial charge transfer (CT) excitons in molecule-TMD heterojunctions enables the electronic structure hybridization between TMD and molecules.[20,21] Recently, CT trions, also referred to as interlayer trions, were also observed in TMD/TMD heterojunctions, offering another route to control and transfer electronic properties across the heterojunctions.[22,23] Given the dramatic difference between electronic structures of molecules and TMD—molecular electronic wavefunctions are much more localized, it is a pertinent question to ask whether the strong many-body interactions that enable CT

trion formations in the TMD/TMD heterojunction can persist if molecules replace a TMD layer to serve as charge acceptors. Realizing CT trions in monolayer-TMD heterojunctions may be able to transfer specific attributes of trions in TMD to the surface molecular species, including spin polarizations to enable spin-polarized chemistry[24–27] and the in-plane delocalization that facilitates charge hopping among molecular sites. In return, the surface molecules could dynamically modify these electronic characteristics in TMD through CT trions, for photonics, optoelectronic and valleytronic applications.

The lack of studies on CT trions at molecule-TMD interfaces stems from the technical challenges to study charge dynamics.[28–32] Photoluminescence (PL) is the predominant optical technique used to investigate monolayer TMD, where the signal can either be enhanced or quenched by molecular doping.[33,34] However, the charge transfer dynamics often occurs on the femtosecond time scale, which is beyond the common time resolution of time-resolved PL. Transient absorption (TA) has also been applied to investigate monolayer TMD,[35–40] interfacial charge transfer between two TMD layers,[41,42] and between TMD and conjugated molecules.[43–45] Yet, it has been not used to study CT trion formation at molecule-TMD interfaces. Interfacial sensitive second harmonic generation (SHG) was also applied on pristine TMD.[46,47] However, its narrow spectral coverage makes SHG difficult to differentiate electronic states, making it unsuitable to identify CT trions.

In this work, we implemented transient electronic sum frequency generation (tr-ESFG) to investigate the ultrafast charge dynamics at a molecule-TMD heterojunction. Tr-ESFG is particularly suitable for this study because of its broad-spectral coverage and surface sensitivity. As a second order nonlinear optic, SFG only occurs for samples with non-centrosymmetric geometries, such as surfaces and interfaces.[48–54] Thus, ESFG has been used to study interfacial molecule alignment[55] and charge dynamics at surfaces/interfaces.[56–61] Using this unique method, we report ultrafast dynamics of photo-induced charge transfer between the heterojunction of monolayer molybdenum disulfide (MoS_2) and ruthenium(ii) polypyridyl complexes (Ru-(DPPZ)$_2$L-Pro), referred as Ru–MoS_2 hereafter. We find that, in contrast to TA, the ground state bleach (GSB) and stimulated emission (SE) of tr-ESFG are out of phase and thereby cancel. This phase cancellation removes the larger ground state signals, promoting the characterization of trion formation timescales. Furthermore, the spectral signal strongly indicates the formation of CT trions at the heterojunction. The identification of a CT-trion in molecule-TMD heterojunctions offers the potential for transferring spin or valley degrees of freedom of TMD to molecules for molecular-based spintronics,[62] spin-specific chemistry,[63,64] and engineering of TMD properties through molecular dopants.[65]

Results and Discussion

A charge transfer interface was created within a type II heterojunction between monolayer MoS_2 and Ru(DPPZ)$_2$L-Pro. Ruthenium(ii) polypyridyl complexes are a group of promising candidates for water oxidation catalyst.[66–68] The hole in Ruthenium(ii) polypyridyl can enhance the efficiency for catalyzing water oxidation (oxygen evolution).[69] Therefore, the heterojunctions comprised of MoS_2 and Ru-(DPPZ)$_2$L-Pro may be developed into photocatalyst based on type II hole transfer, taking advantage of the exceptional characteristics of monolayer TMD, including large absorption cross section and valley degrees of freedom, and the catalytic nature of the Ruthenium(ii) polypyridyl complexes. Based on a combination of UV/Vis absorption, PL, and cyclic voltammetry measurements, (see supplemental Figure S5, Figure S6), we find that the HOMO of Ru-(DPPZ)$_2$L-Pro lies above the MoS_2 valance band maximum (VBM)[70] while the LUMO is higher than the conduction band minimum (CBM)[70] of MoS_2, as described in Figure 1, facilitating the hole transfer from monolayer MoS_2 to the molecule upon photoexcitation.

The efficient interfacial charge transfer between monolayer MoS_2 and Ru(DPPZ)$_2$L-Pro was confirmed by the quenching of Ru–MoS_2 PL signals (Figure 2a). Optical microscope shows an image for a pristine MoS_2 flake containing a large area of monolayer MoS_2 and minor part for bilayer MoS_2 and bulk MoS_2 (Figure 2b). For pristine

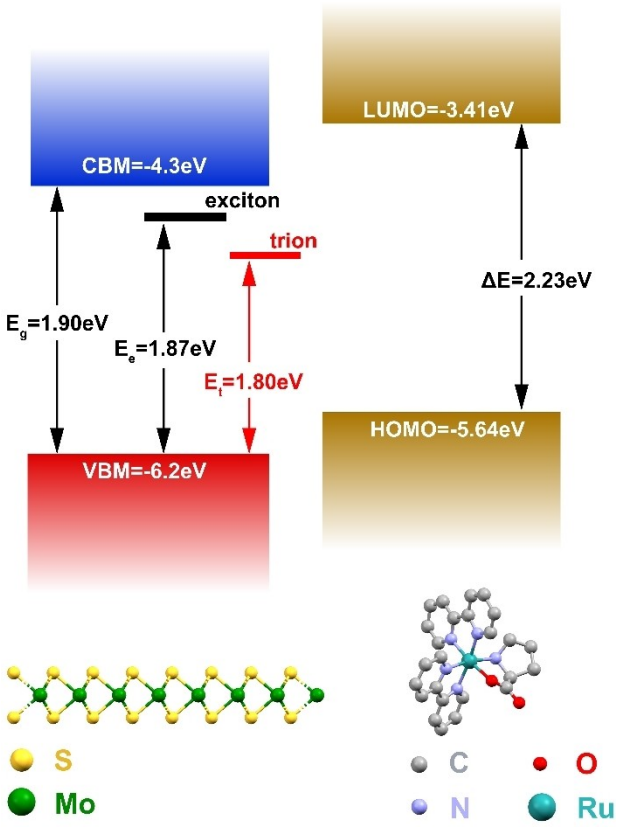

Figure 1. band alignment of Ru–MoS_2 heterojunction

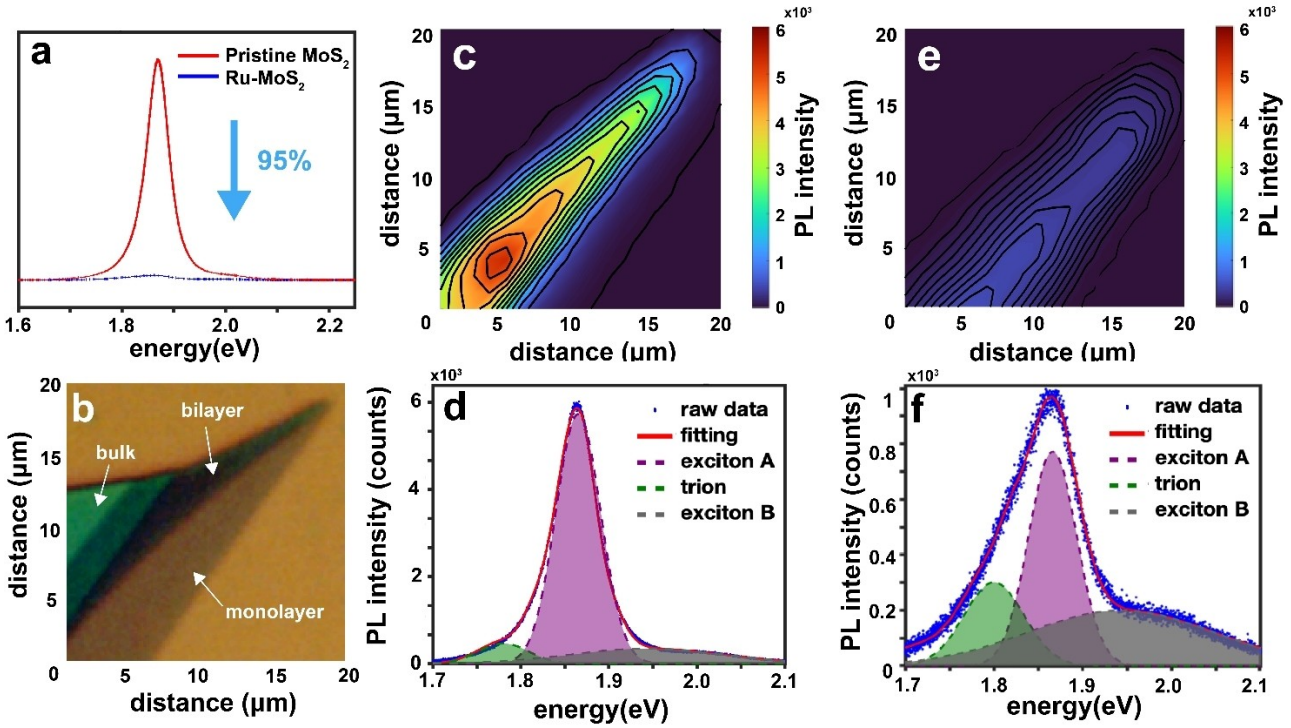

Figure 2. Photoluminescent result to confirm interfacial charge transfer. (a) PL spectrum comparison on a typical position of monolayer MoS_2, 95% quenching effect after Ru(DPPZ)$_2$L-Pro doped; (b) 20 μm by 20 μm optical image of monolayer MoS_2 flake ; (c) PL microscope mapping on same pristine monolayer MoS_2, higher PL intensity at left corner is due to dominated signal from monolayer, while the top area contains both signal from monolayer and multilayer sample (beam size of PL is 4 μm as diameter) leading to a lower intensity;(d) fitting result for PL spectrum of pristine monolayer MoS_2; (e) PL microscope mapping on Ru–MoS_2; (f) fitting result of Ru–MoS_2

monolayer MoS_2, the PL mapping (Figure 2c) at 690 nm presents a uniform signal intensity, indicating a highly homogeneous material. The PL spectrum of the pristine sample (Figure 2d) can be decomposed into three gaussian peaks: the radiative recombination of B-exciton, A-exciton and negative trion, at 2.00, 1.87, and 1.78 eV, respectively.[71]

Exciton A and B are formed by strong spin orbital coupling (SOC) that leads to a split in highest valence band of ~130 meV. The trion, with a larger coulomb binding energy, is identified at a lower energy, in good agreement with the literatures.[27] Upon functionalizing the monolayer MoS_2 by Ru(DPPZ)$_2$L-Pro, the PL emission was quenched by 95% uniformly across the entire monolayer MoS_2 surface, as shown in Figure 2a and e. All three of the spectra components are reduced in Figure 2f, suggesting all three quasiparticles are subject to interfacial charge transfer. We note that the signal reduction is unlikely to be attributed to the absorbance of the excitation lights by the surface adsorbed Ru(DPPZ)$_2$L-Pro layer, as evidenced by the absence of absorption within the excitation wavelength range from a pure Ru(DPPZ)$_2$L-Pro layer (see supplemental Section 10). Thus, an interfacial charge transfer occurs at the Ru–MoS_2 interface.

Although the existence of charge transfer was confirmed, the mechanism and dynamics of the interfacial charge transfer and whether CT trion could exist at the interfaces remain unknown. To elucidate these, we applied Tr-ESFG spectroscopy. A 515 nm (2.4 eV, 200 fs) pump pulse excites electrons to the conduction band of monolayer MoS_2 (E_g = 1.9 eV). The subsequent charge dynamics are then probed by the ESFG (Figure 3a). The ESFG probe utilizes a mid-IR and near-IR pulses to interact with the sample which creates a signal at the sum of the two incoming beam frequencies.[72,73] If the energy of the emitted signal resonates with an electronic transition at interfaces, the emitted signal is enhanced (inset of Figure 3a). We scanned the IR frequency across a broad spectral range to cover the electronic transitions.

The static ESFG spectrum in Figure 3b of pristine monolayer MoS_2 and Ru–MoS_2 show large peaks around 1.77–1.78 eV which are assigned to be the ESFG resonances of trions, based on the PL fitting in Figure 2 and UV-Vis absorption features in supplement Figure S6b. Interestingly, monolayer MoS_2 has a higher ESFG peak intensity than Ru–MoS_2 sample, indicating a decrease of transition from ground to trion states after doping. This decrease suggests the interfacial electronic structures have been modified, so that the transition probabilities of excitons and trions are changed. We note because monolayer MoS_2 emits strong PL signals at 1.9 eV, it interferes with ESFG signal of the exciton A. For this reason, we focus on trion charge transfer mechanism to infer the complete charge transfer picture.

The tr-ESFG spectra of pristine monolayer MoS_2 and Ru–MoS_2 show distinct time-dependent features. At first glance, pristine TMD (see Figure 3c) exhibits a negative pump-probe signal right after time zero and recovers back

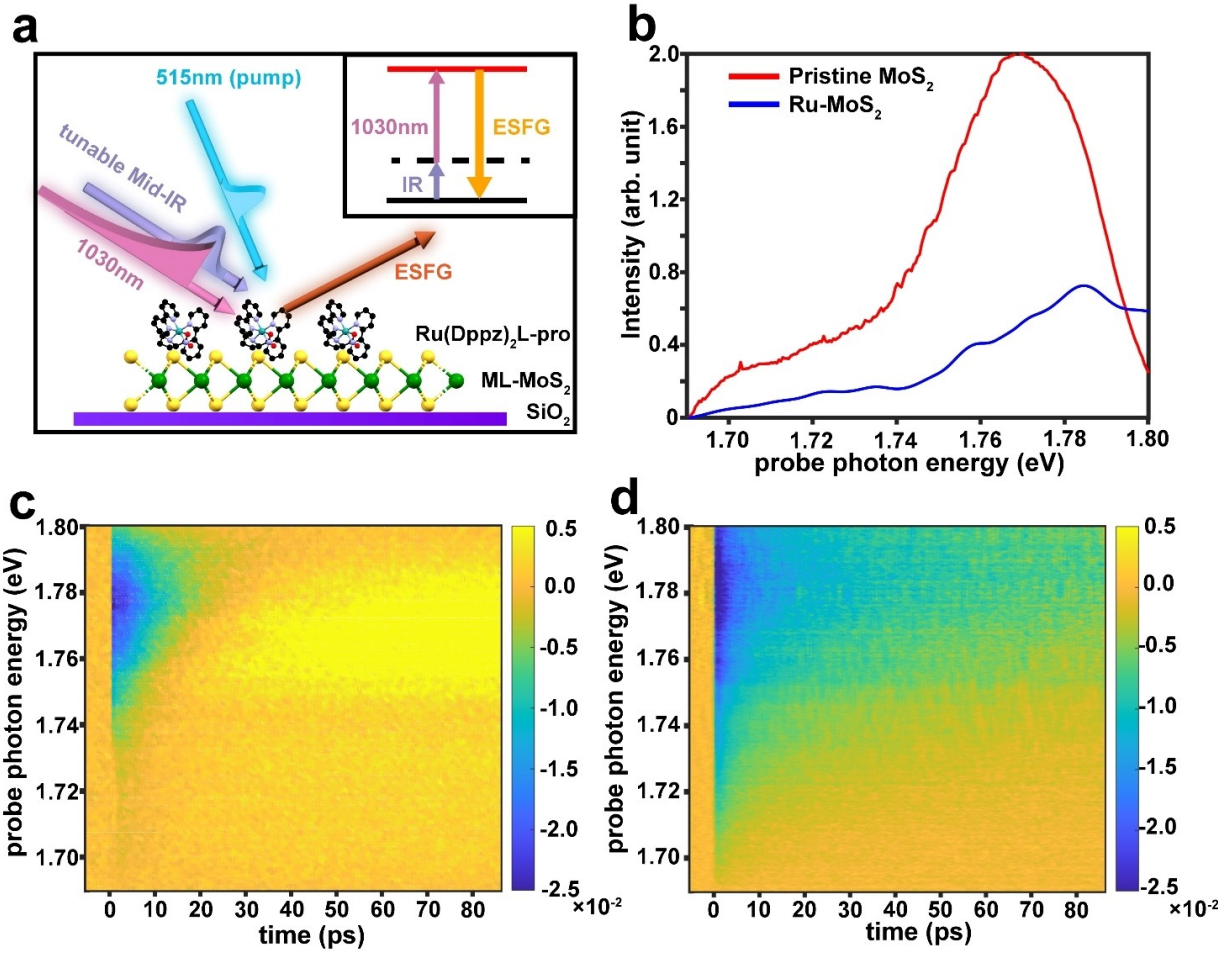

Figure 3. transient ESFG measurements of Ru–MoS_2 heterojunction and pristine monolayer MoS_2 samples (a) illustration Figure of Tr-ESFG; (b) static ESFG of pristine monolayer MoS_2 and Ru–MoS_2 with no optical pumping; (c) Pseudo color 2D tr-ESFG spectrum pristine monolayer MoS_2; (d) Pseudo color 2D tr-ESFG spectrum Ru–MoS_2. The color bar in (c) and (d) represents the intensity of pump probe data. The yellow (blue) color represents a positive (negative) tr-ESFG signal (sample emits stronger (weaker) ESFG after being pumped). The mathemstical description of how to calculate tr-ESFG is shown in supplement section 2.

to zero with a lifetime of 16.4 ps before turning into a positive amplitude with a long lifetime of 129.0 ps. The negative transient signal has a center located at 1.79 eV, indicating a bleach of trion.

Interestingly, the positive signal redshifts to 1.76Ev. For the Ru–MoS_2 (Figure 3d), a negative signal persists over the entire scanning range and only decays to a smaller amplitude. We note the Ru(DPPZ)$_2$L-pro monolayer alone shows negligible static and transient ESFG signal (see supplement Figure S12).

Origins of Tr-ESFG Signals

To understand the tr-ESFG dynamics of pristine monolayer MoS_2 and Ru–MoS_2, it is necessary to dive into the origins of tr-ESFG, which, as shown below, has different spectral features than the more commonly applied TA spectroscopy. For a full theoretical treatment,[74–76] we refer to Supporting Information Section 11. Briefly, similar to TA, there are three contributions to the tr-ESFG signals, i.e. ground state bleach, stimulated emission and excited state absorption, where the excited state absorption is always shifted relative to the other two due to particle interactions. However, different from TA, whose ground state bleach and stimulated emission signals have the same phase and thereby often add up and dominate the TA features—masking other features, in tr-ESFG, ground state bleach and stimulated emission have opposite phases and cancel each other, allowing other important but subtle features to be analyzed.

The origin of the phase difference can be intuitively understood by that tr-ESFG measures changes of ESFG emission, whereas TA quantifies the modulations of absorptions. As a result, stimulated emision enhances the ESFG emission, but reduces the amount of absorption in TA. Below, we show that this cancelation allows us to better quantify the trion dynamics.

Charge Dynamics of Pristine Monolayer MoS_2

This opposite phase relationship between ground state bleach and stimulated emission provides advantages in analyzing the measured spectral dynamics. A typical monolayer MoS_2 photoexcitation and relaxation process[77,78] is described in Figure 4a. The electron is photoexcited from the valence band to the conduction band and excitons are formed. An exciton and an extra electron can further combine to form trions at a lower energy state (with a rate constant k_1), which occurs at 10–20 ps according to literatures.[79,80]

Lastly, trion recombination occurs with a rate constant of k_2. Based on this kinetic model, the transient population of each state can be described as,

$$\begin{cases} \Delta[E]_{(t)} = E_0 e^{-k_1 t} \\ \Delta[T]_{(t)} = \frac{E_0 k_1}{k_1 - k_2} e^{-k_2 t} - \frac{E_0 k_1}{k_1 - k_2} e^{-k_1 t} \\ \Delta[G]_{(t)} = -\frac{E_0 k_1}{k_1 - k_2} e^{-k_2 t} + \frac{E_0 k_2}{k_1 - k_2} e^{-k_1 t} \end{cases} \quad (1)$$

where E_0 is the initial exciton population at $t=0$. The ground state bleach and stimulated emission are at the same trion emission frequency, so their signals need to be combined. Based on the harmonic oscillator approximation, they emit at the same intensity,[81] and the combined signal leads to a cancelation of the dynamics related to k_2,

$$I_{GSB+SE} \propto \Delta[G]_{(t)} + \Delta[T]_{(t)} = -E_0 e^{-k_1 t} \quad (2)$$

Thus, the ground state bleach and stimulated emission spectra are only sensitive to the relaxation from excitons to trions. For excited state absorption, it is expected that it emits at a lower energy due to the binding energy between trions, and its dynamic should reflect the trion population.

$$I_{ESA} \propto \Delta[T]_{(t)} = \left(\frac{E_0 k_1}{k_1 - k_2} e^{-k_2 t} - \frac{E_0 k_1}{k_1 - k_2} e^{-k_1 t} \right) \quad (3)$$

The tr-ESFG of pristine monolayer MoS_2 is therefore composed of two components, one spectral component corresponding to the combined ground state bleach and stimulated emission signal, described by a single exponential, and the other spectral component corresponding to excited state absorption, described by double exponentials. We therefore apply a Global Analysis to the raw data of Figure 3b using the two-component model described by Eq. 2&3. The extracted earlier negative signal represents the combination of ground state bleach and stimulated emission, described by the red spectrum in Figure 4b. It has a lifetime of 16.4±0.5 ps ($k_1 = 0.061\ ps^{-1}$), corresponding the exciton to trion relaxation timescale.[82,83] This negative spectral feature can be intuitively viewed as a state-blocking effect from the trion, which commonly exists in TA. The positive feature appears later is excited state absorption, which has a biexponential dynamic, agreeing with our model. This signal rises with the rate constant of k_1 and decays with a long lifetime of 129±20 ps ($k_2 = 0.0078\ ps^{-1}$, Figure 4c). Interestingly, this excited state absorption signal peaks at 1.76 eV, indicating a 0.02–0.03 eV energy reduction due to the interaction between trions. This binding energy is smaller than bi-excitons.[84]

Charge Transfer Dynamics of Ru–MoS_2 Heterojunction

We proceed to analyze the transient dynamics of Ru–MoS_2 monolayer. In comparison to the pristine MoS_2, a negative transient signal emerges at an early time, still indicative of the ground state bleach and stimulated emission signal contributions—the state-blocking effect remains. However, the lack of the positive signal after 10 ps implies negligible excited state absorption signal, indicating no trion formation, which agrees with the suppression of PL signals from trions (Figure 2c). The band alignment of the heterojunction suggests that a hole transfer from the valence band of MoS_2 to the HOMO of $Ru(DPPZ)_2L\text{-}Pro$ is energetically favorable, eliminating the trion population.

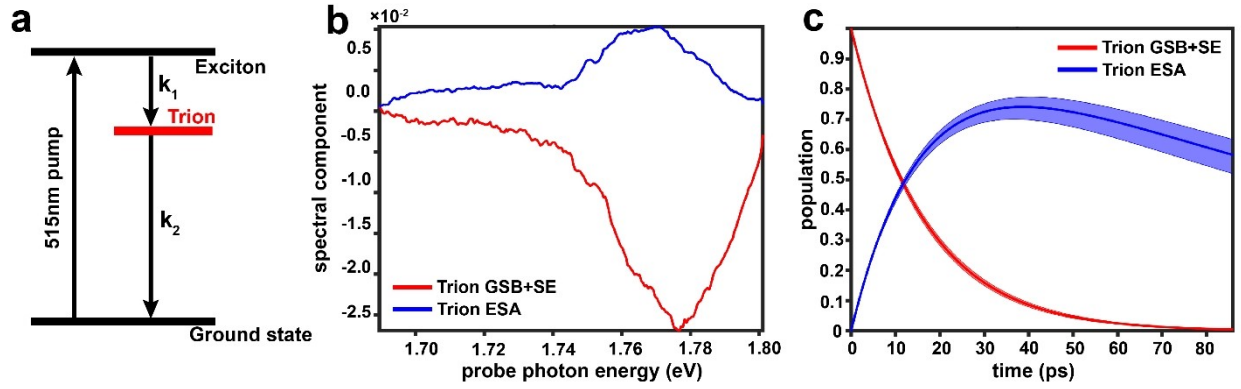

Figure 4. tr-ESFG data analysis of monolayer MoS_2. (a) Kinetic model for monolayer MoS_2. (b) spectra components from global analysis of pristine monolayer MoS_2. (c) Population dynamics from global analysis of monolayer MoS_2, for trion GSB+SE, lifetime is 16.4±0.548 ps; for trion ESA, lifetime is 129.0±18.48 ps. Solid line shows the best fitting result, while shaded area shows the confidence range of the fitting.

A trion in a monolayer TMD forms when a photogenerated electron-hole pair (or exciton) bonds with another free electron in the TMD conduction band. At the molecule-TMD interface, after the hole transfers to the molecule, two electrons remain in the TMD. There are different potential pathways for these three charge carriers to interact and relax after this interfacial charge transfer: 1. The holes and electrons are separated into two free electrons and one free hole. This process creates an excess unpaired electron in the conduction band of TMD due to photoexcitation, which are now available to form additional trions in TMDs. Thus, this scenario should enhance the ESFG signal of trion transitions—creating a positive transient signal, which is opposite from the measured transient decrease of ESFG signals. 2. An electron and one transferred hole remain tightly bonded, forming a CT exciton. This case leaves the other electron in the original trion to be a free electron in the conduction band, no extra free electron compared to the case without optical pumping, which should lead to no tr-ESFG signals. 3. Two electrons in the conduction band of monolayer MoS_2 and one hole in $Ru(DPPZ)_2$L-Pro bind into a CT-trion. This case leaves one less free electron in the conduction band of monolayer MoS_2, leading to a transient negative ESFG signal. Only the last scenario agrees with the experimental observation of a decreased transient ESFG signals. As a result, we assigned the long-lasting negative transient ESFG signal to the bleaching of the regular trion due to the CT trion formation, which retains the state-blocking effects seen in the trion case in pure monlayer MoS_2. We note that to measure the CT trions directly, it is necessary to shift the IR spectral range to 9 μm, which is out of the practical range for our instrument. To further examine this CT trion assignments, we have conducted additional wavelength dependent PL measurements and control experiments of tr-ESFG of bare Ru $Ru(DPPZ)_2$L-Pro layer (SI section 3 and section 10).

We, therefore, add a competing pathway of CT trion formation to the MoS_2 kinetic model. (see in Figure 5 and Supporting Information Section 13) Sequential model (exciton→trion→CT-trions) is not chosen because of the absence of trion signals in this sample. Using the parallel kinetic model, the negative signal at 1.78 eV can be expressed as summation of ground state bleach and stimulated emission:

$$I_{negative\ signal} = I_{GSB} + I_{SE} \sim \Delta[G]_{(t)} + \Delta[T]_{(t)} = \frac{E_0(k_1k_2 - k_2k_4 + k_3k_4 - k_1k_3 + k_1k_4 - k_1^2)}{(k_1 - k_2 + k_3)(k_1 + k_3 - k_4)} e^{-(k_1+k_3)t} - \frac{E_0k_3}{k_1 + k_3 - k_4} e^{-k_4t} \quad (4)$$

The described model suggests that the transient signal should be a bi-exponential decay, with the dynamics independent of frequency because only one spectral component should exist. We confirm this prediction by fitting dynamics traces at various frequencies into a biexponential decay. We find a fast decay with $(k_1 + k_3)^{-1} = 5.6$ ps and a long-lived decay with $k_4^{-1} = 90.9$ ps regardless of the probing frequency (Figure 5b). The conclusion is further supported by a global analysis (See Supplemental Figure S15): if we decompose the spectra into two spectral/dynamical components, both components exhibit identical spectra features. The results, therefore, indicate only a single spectral component exists with a biexponential decay, agreeing with our kinetic model.

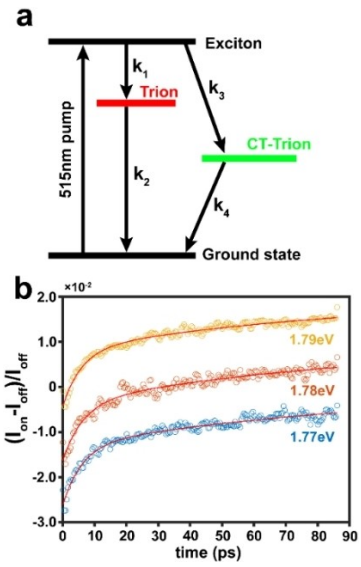

Figure 5. tr-ESFG data analysis of Ru–MoS_2 heterojunctions. (a) a schematic of kinetic model for the Ru–MoS_2 heterojunction. The horizontal bars represent energy levels (esimation is based on the band alignment of heterojunction, supplement Section 4 and 5); (b) Bi-exponential fitting for pump-probe signal at a certain frequency. A 0.01 offset is applied between different energies for a clear visualization. At different probe photon energies, the bi-exponential fitting has a similar result of fast decay with 5.6 ps and slow decay with 90.9 ps.

With the validated kinetic model, we proceed to determine the $k_1$and k_3 from the spectra results. Because there is a negligible excited state absorption signal in the tr-ESFG, it indicates no or little population of trion in the measured time window, i.e., $\Delta[T] \approx 0$, suggesting that k_1 is negligible comparing to k_3. Thus, $k_3^{-1} \approx (k_1 + k_3)^{-1} = 5.6$ ps.The formation of CT-trion dominates the exciton relaxation and quenches the original trion formation.

Mechanism of CT-trion Formation

Based on control experiments in Supplement Section 9, the $Ru(DPPZ)_2$L-pro prefers to bind to defect sites, forming a localized hole acceptor. Therefore, the mechanism of CT-trion formation is: After being photoexcited, a hole from valence band of MoS_2 transfers to the localized HOMO orbital. Meanwhile, the electrons in conduction band of MoS_2 cool down and bind to the transferred hole by the strong coulomb attraction to form a CT-trion. (Figure 6)

Based on these insights, we discuss the conditions of forming CT-trions at TMD/molecule heterojunctions. First, the appropriate charge transfer needs to occur. For the

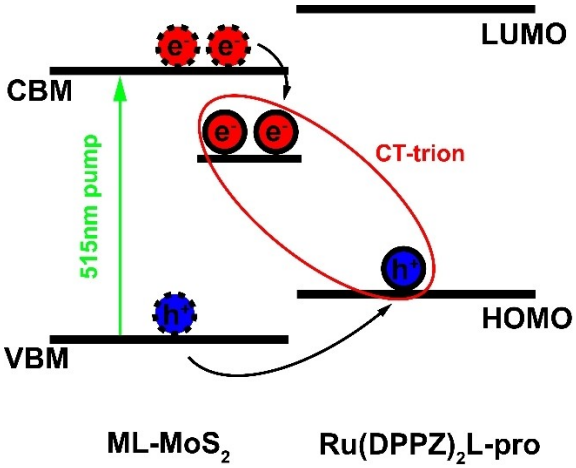

Figure 6. Schematic of CT-trion formation and charge transfer process.

current systems, the trion in TMD is a negative trion (extra electrons on conduction bands plus an exciton). In this case, compared to an electron transfer, a hole transfer maximally preserved the interactions for trion formations. In contrast, should the adsorbed molecule facilitate electron transfer, it may result in an exciton in TMD and an extra free electron in molecules, as predicted by a theoretical study of a MoS_2/WS_2.[85] Thus, hole (electron) transfer is best to maintain CT trion for negative (positive) trions.

Second, after charge transfer, the electron-hole attractions should be preserved to form trions, which appears to be the case here. This result suggested that the screening from TMD/molecular heterojunction interfaces is small enough to maintain a large electron-hole attraction. We hypothesize that this is due to the localized nature of the molecules, the TMD structures are minimally disrupted, in sharp contrast to TMD/TMD or bulk TMD, where large screening exists. Thus, the TMD/molecule heterojunction largely preserved the low screening character of the 2D monolayer materials, allowing the electric fields between electrons and holes to penetrate low dielectric media, such as vacuum (the so-called dielectric confinement effect[86]), without much screening.

Lastly, we note that the lifetime of CT trions appears to be shorter than the regular trions, which contradicts with conventional assumption that the separation of charge carriers would suppress their recombination and prolong the bound electron-hole complex lifetime. The shorten lifetime indicates that the localized HOMO orbital acts as a 0-D hole trap, possibly due to a strong covalent binding, leading to a tightly bonded local trion near the molecule.[87] The reduced dimensionality leads to a smaller exciton Bohr radius[88–90] resulting in a larger trion binding energy[91–95] and faster trion formation time.[87,92,93,96]

Conclusion

In this study, we apply the unique transient ESFG to characterize charge transfer between heterojunction of monolayer MoS_2 and ruthenium(ii) polypyridyl complexes. We show that transient ESFG has a different sensitivity to trion dynamics compared to TA. The long-lasting bleach signal and lack of positive peaks in transient ESFG spectra of Ru–MoS2, in comparison to the one of pristine MoS_2, strongly suggests the formation of CT-trions, resulting from the interfacial hole transfer from MoS_2 to the molecular adsorbates. The fast formation time (5.6 ps) showcases a very efficient CT-trion generation attributed to the reduced dimensionality, and that CT-trion dominates over regular trion at molecule-TMD interfaces. The dominance of CT trions opens the possibility to transfer many-body physics unique to TMD materials to the surface adsorbed molecules, leading to engineering surface molecules with unconventional catalytic performance. In return, molecular doping provides a new way to control many-body interactions of TMD. For example, by functionalizing specific areas of TMD with molecules, it can enable local electronic structures and dynamics engineering.

Supporting Information

The authors have cited additional references within the Supporting Information (Refs. [97–102]).

Acknowledgements

The authors thank Dr. Haochuan Mao, Dr. Wenfan Chen and Dr. Chun-Chieh Yu for their valuable discussion in the manuscript. The authors thank Alyssa F. Cavazos for her help in preparing the manuscript. Y.J., N.M., C.W. and W. X., and S.K.C. are supported by a collaborative grant from Department of Energy DE-FOA-0002449. K.L., H.Z. and Z.L. and S.L. are supported by NSF under the grant CHE-2303936 awarded to S.L. Z.S. was supported by ERC-CZ program (project LL2101) from Ministry of Education Youth and Sports (MEYS) and by the project Advanced Functional Nanorobots (reg. No. CZ.02.1.01/0.0/0.0/15_003/0000444 financed by the EFRR). J.P., J.S. and C.P.K. are supported by NSF under the grant CHE-1853908 and CHE-2153757 awarded to C.P.K.

Conflict of Interest

The authors declare no conflict of interest.

Data Availability Statement

The data that support the findings of this study are openly available in GITHUB at https://github.com/EthanJing1/Rawdata_Ru_MoS2.git.

Keywords: charge transfer · trion · Time-resolved interfacial-sensitive spectroscopy · sum frequency generation · molecular- functionalized monolayer TMD

[1] M. Kan, J. Y. Wang, X. W. Li, S. H. Zhang, Y. W. Li, Y. Kawazoe, Q. Sun, P. Jena, *J. Phys. Chem. C* **2014**, *118*, 1515–1522.

[2] N. Alidoust, G. Bian, S. Y. Xu, R. Sankar, M. Neupane, C. Liu, I. Belopolski, D. X. Qu, J. D. Denlinger, F. C. Chou, M. Z. Hasan, *Nat. Commun.* **2014**, *5*, DOI 10.1038/ncomms5673.

[3] D. Vaquero, V. Clericò, J. Salvador-Sánchez, A. Martín-Ramos, E. Díaz, F. Domínguez-Adame, Y. M. Meziani, E. Diez, J. Quereda, *Commun. Phys.* **2020**, *3*, DOI 10.1038/s42005-020-00460-9.

[4] K. F. Mak, K. He, C. Lee, G. H. Lee, J. Hone, T. F. Heinz, J. Shan, *Nat. Mater.* **2013**, *12*, 207–211.

[5] W. Wang, N. Sui, M. Ni, X. Chi, L. Pan, H. Zhang, Z. Kang, Q. Zhou, Y. Wang, *J. Phys. Chem. C* **2020**, *124*, 1749–1754.

[6] A. Ayari, E. Cobas, O. Ogundadegbe, M. S. Fuhrer, *J. Appl. Phys.* **2007**, *101*, DOI 10.1063/1.2407388.

[7] B. Radisavljevic, A. Radenovic, J. Brivio, V. Giacometti, A. Kis, *Nat. Nanotechnol.* **2011**, *6*, 147–150.

[8] S. Kallatt, S. Das, S. Chatterjee, K. Majumdar, *NPJ 2D Mater. Appl.* **2019**, *3*, DOI 10.1038/s41699-019-0097-3.

[9] H. Lee, Y. Koo, S. Kumar, Y. Jeong, D. G. Heo, S. H. Choi, H. Joo, M. Kang, R. H. Siddique, K. K. Kim, H. S. Lee, S. An, H. Choo, K. D. Park, *Nat. Commun.* **2023**, *14*, DOI 10.1038/s41467-023-37481-1.

[10] R. Liu, F. Wang, L. Liu, X. He, J. Chen, Y. Li, T. Zhai, *Small Structures* **2021**, *2*, DOI 10.1002/sstr.202000136.

[11] S. J. Liang, B. Cheng, X. Cui, F. Miao, *Adv. Mater.* **2020**, *32*, DOI 10.1002/adma.201903800.

[12] S. Zhang, J. Liu, M. M. Kirchner, H. Wang, Y. Ren, W. Lei, *J. Phys. D* **2021**, *54*, DOI 10.1088/1361-6463/ac16a4.

[13] Z. Song, T. Schultz, Z. Ding, B. Lei, C. Han, P. Amsalem, T. Lin, D. Chi, S. L. Wong, Y. J. Zheng, M. Y. Li, L. J. Li, W. Chen, N. Koch, Y. L. Huang, A. T. S. Wee, *ACS Nano* **2017**, *11*, 9128–9135.

[14] S. Bertolazzi, M. Gobbi, Y. Zhao, C. Backes, P. Samorì, *Chem. Soc. Rev.* **2018**, *47*, 6845–6888.

[15] Y. Huang, F. Zhuge, J. Hou, L. Lv, P. Luo, N. Zhou, L. Gan, T. Zhai, *ACS Nano* **2018**, *12*, 4062–4073.

[16] S. Andleeb, X. Wang, H. Dong, S. Valligatla, C. N. Saggau, L. Ma, O. G. Schmidt, F. Zhu, *Nanomaterials* **2023**, *13*, DOI 10.3390/nano13091491.

[17] S. Li, C. Zhong, A. Henning, V. K. Sangwan, Q. Zhou, X. Liu, M. S. Rahn, S. A. Wells, H. Y. Park, J. Luxa, Z. Sofer, A. Facchetti, P. Darancet, T. J. Marks, L. J. Lauhon, E. A. Weiss, M. C. Hersam, *ACS Nano* **2020**, *14*, 3509–3518.

[18] M. Van Winkle, I. M. Craig, S. Carr, M. Dandu, K. C. Bustillo, J. Ciston, C. Ophus, T. Taniguchi, K. Watanabe, A. Raja, S. M. Griffin, D. K. Bediako, *Nat. Commun.* **2023**, *14*, DOI 10.1038/s41467-023-38504-7.

[19] R. Hou, Y. Xia, S. Yang, *ACS Omega* **2020**, *5*, 26748–26754.

[20] T. R. Kafle, B. Kattel, S. D. Lane, T. Wang, H. Zhao, W. L. Chan, *ACS Nano* **2017**, *11*, 10184–10192.

[21] Z. Wang, C. Sun, X. Xu, Y. Liu, Z. Chen, Y. M. Yang, H. Zhu, *J. Am. Chem. Soc.* **2023**, *145*, 11227–11235.

[22] L. Zhang, F. Zhou, X. Zhang, S. Yang, B. Wen, H. Yan, T. Yildirim, X. Song, Q. Yang, M. Tian, N. Wan, H. Song, J. Pei, S. Qin, J. Zhu, S. Wageh, O. A. Al-Hartomy, A. G. Al-Sehemi, H. Shen, Y. Liu, H. Zhang, *Adv. Mater.* **2023**, *35*, DOI 10.1002/adma.202206212.

[23] T. Deilmann, K. S. Thygesen, *Nano Lett.* **2018**, *18*, 1460–1465.

[24] M. Chhowalla, H. S. Shin, G. Eda, L. J. Li, K. P. Loh, H. Zhang, *Nat. Chem.* **2013**, *5*, 263–275.

[25] Z. Wang, L. Zhao, K. F. Mak, J. Shan, *Nano Lett.* **2017**, *17*, 740–746.

[26] M. Chhowalla, Z. Liu, H. Zhang, *Chem. Soc. Rev.* **2015**, *44*, 2584–2586.

[27] X. Xu, W. Yao, D. Xiao, T. F. Heinz, *Nat. Phys.* **2014**, *10*, 343–350.

[28] M. R. Habib, H. Li, Y. Kong, T. Liang, S. M. Obaidulla, S. Xie, S. Wang, X. Ma, H. Su, M. Xu, *Nanoscale* **2018**, *10*, 16107–16115.

[29] X. Zhu, N. R. Monahan, Z. Gong, H. Zhu, K. W. Williams, C. A. Nelson, *J. Am. Chem. Soc.* **2015**, *137*, 8313–8320.

[30] X. Zhu, N. R. Monahan, Z. Gong, H. Zhu, K. W. Williams, C. A. Nelson, *J. Am. Chem. Soc.* **2015**, *137*, 8313–8320.

[31] S. Das, Y. Wang, Y. Dai, S. Li, Z. Sun, *Light-Sci. Appl.* **2021**, *10*, DOI 10.1038/s41377-021-00462-4.

[32] N. Kumar, J. He, D. He, Y. Wang, H. Zhao, *J. Appl. Phys.* **2013**.

[33] I. Irfan, S. Golovynskyi, M. Bosi, L. Seravalli, O. A. Yeshchenko, B. Xue, D. Dong, Y. Lin, R. Qiu, B. Li, J. Qu, *J. Phys. Chem. C* **2021**, *125*, 4119–4132.

[34] J. Choi, H. Zhang, J. H. Choi, *ACS Nano* **2016**, *10*, 1671–1680.

[35] S. Das, Y. Wang, Y. Dai, S. Li, Z. Sun, *Light-Sci. Appl.* **2021**, *10*, DOI 10.1038/s41377-021-00462-4.

[36] P. Valencia-Acuna, P. Zereshki, M. M. Tavakoli, J. H. Park, J. Kong, H. Zhao, *Phys. Rev. B* **2020**, *102*, DOI 10.1103/PhysRevB.102.035414.

[37] Y. Li, X. Wu, W. Liu, H. Xu, X. Liu, *Appl. Phys. Lett.* **2021**, *119*, DOI 10.1063/5.0060587.

[38] C. Cheng, J. Zhang, B. Zhu, G. Liang, L. Zhang, J. Yu, *Angew. Chem. Int. Ed.* **2023**, *62*, DOI 10.1002/anie.202218688.

[39] R. Canton-Vitoria, H. B. Gobeze, V. M. Blas-Ferrando, J. Ortiz, Y. Jang, F. Fernández-Lázaro, Á. Sastre-Santos, Y. Nakanishi, H. Shinohara, F. D'Souza, N. Tagmatarchis, *Angew. Chem.* **2019**, *131*, 5768–5773.

[40] I. K. Sideri, Y. Jang, J. Garcés-Garcés, Á. Sastre-Santos, R. Canton-Vitoria, R. Kitaura, F. Fernández-Lázaro, F. D'Souza, N. Tagmatarchis, *Angew. Chem. Int. Ed.* **2021**, *60*, 9120–9126.

[41] X. Hong, J. Kim, S. F. Shi, Y. Zhang, C. Jin, Y. Sun, S. Tongay, J. Wu, Y. Zhang, F. Wang, *Nat. Nanotechnol.* **2014**, *9*, 682–686.

[42] S. B. Homan, V. K. Sangwan, I. Balla, H. Bergeron, E. A. Weiss, M. C. Hersam, *Nano Lett.* **2017**, *17*, 164–169.

[43] S. B. Homan, V. K. Sangwan, I. Balla, H. Bergeron, E. A. Weiss, M. C. Hersam, *Nano Lett.* **2017**, *17*, 164–169.

[44] C. Zhong, V. K. Sangwan, C. Wang, H. Bergeron, M. C. Hersam, E. A. Weiss, *J. Phys. Chem. Lett.* **2018**, *9*, 2484–2491.

[45] S. Padgaonkar, S. H. Amsterdam, H. Bergeron, K. Su, T. J. Marks, M. C. Hersam, E. A. Weiss, *J. Phys. Chem. C* **2019**, *123*, 13337–13343.

[46] A. Autere, H. Jussila, A. Marini, J. R. M. Saavedra, Y. Dai, A. Säynätjoki, L. Karvonen, H. Yang, B. Amirsolaimani, R. A. Norwood, N. Peyghambarian, H. Lipsanen, K. Kieu, F. J. G. De Abajo, Z. Sun, *Phys. Rev. B* **2018**, *98*, DOI 10.1103/PhysRevB.98.115426.

[47] L. Mennel, M. Paur, T. Mueller, *APL Photonics* **2019**, *4*, DOI 10.1063/1.5051965.

[48] Y. R. Shen, V. Ostroverkhov, *Chem. Rev.* **2006**, *106*, 1140–1154.

[49] M. Vinaykin, A. V. Benderskii, *J. Phys. Chem. Lett.* **2012**, *3*, 3348–3352.

[50] Y. Tong, Y. Zhao, N. Li, M. Osawa, P. B. Davies, S. Ye, *J. Chem. Phys.* **2010**, *133*, DOI 10.1063/1.3428668.

[51] P. E. Ohno, H. F. Wang, F. Paesani, J. L. Skinner, F. M. Geiger, *J. Phys. Chem. A* **2018**, *122*, 4457–4464.

[52] J. Tan, B. Zhang, Y. Luo, S. Ye, *Angew. Chem. Int. Ed.* **2017**, *56*, 12977–12981.

[53] M. Bonn, Y. Nagata, E. H. G. Backus, *Angew. Chem.* **2015**, *127*, 5652–5669.

[54] J. Lu, A. Carvalho, H. Liu, S. X. Lim, A. H. Castro Neto, C. H. Sow, *Angew. Chem.* **2016**, *128*, 12124–12128.
[55] S. Yamaguchi, T. Tahara, *J. Chem. Phys.* **2008**, *129*, DOI 10.1063/1.2981179.
[56] G. H. Deng, Y. Qian, Y. Rao, *J. Chem. Phys.* **2019**, *150*, DOI 10.1063/1.5063458.
[57] D. E. Cotton, A. P. Moon, S. T. Roberts, *J. Phys. Chem. C* **2020**, *124*, 11401–11413.
[58] Y. Li, J. Wang, W. Xiong, *J. Phys. Chem. C* **2015**, *119*, 28083–28089.
[59] G.-H. Deng, Y. Qian, T. Zhang, J. Han, H. Chen, Y. Rao, *The Proceedings of the National Academy of Sciences* **2021**, DOI 10.1073/pnas.2100608118/-/DCSupplemental.
[60] R. De, N. A. Calvet, B. Dietzek-Ivansic, *Angew. Chem. Int. Ed.* **2024**, DOI 10.1002/anie.202313574.
[61] C. Wang, Y. Jing, L. Chen, W. Xiong, *J. Phys. Chem. Lett.* **2022**, *13*, 8733–8739.
[62] A. Forment-Aliaga, E. Coronado, *Chem. Rec.* **2018**, *18*, 737–748.
[63] J. R. Schaibley, H. Yu, G. Clark, P. Rivera, J. S. Ross, K. L. Seyler, W. Yao, X. Xu, *Nat. Rev. Mater.* **2016**, *1*, DOI 10.1038/natrevmats.2016.55.
[64] E. C. Ahn, *NPJ 2D Mater. Appl.* **2020**, *4*, DOI 10.1038/s41699-020-0152-0.
[65] Y. Zhao, K. Xu, F. Pan, C. Zhou, F. Zhou, Y. Chai, *Adv. Funct. Mater.* **2017**, *27*, DOI 10.1002/adfm.201603484.
[66] L. Tong, R. P. Thummel, *Chem. Sci.* **2016**, *7*, 6591–6603.
[67] L. Tong, R. Zong, R. Zhou, N. Kaveevivitchai, G. Zhang, R. P. Thummel, *Faraday Discuss.* **2015**, *185*, 87–104.
[68] H. W. Tseng, R. Zong, J. T. Muckerman, R. Thummel, *Inorg. Chem.* **2008**, *47*, 11763–11773.
[69] I. Purnama, Salmahaminati, M. Abe, M. Hada, Y. Kubo, J. Y. Mulyana, *Dalton Trans.* **2019**, *48*, 688–695.
[70] M. Berg, K. Keyshar, I. Bilgin, F. Liu, H. Yamaguchi, R. Vajtai, C. Chan, G. Gupta, S. Kar, P. Ajayan, T. Ohta, A. D. Mohite, *Phys. Rev. B* **2017**, *95*, DOI 10.1103/PhysRevB.95.235406.
[71] S. Mouri, Y. Miyauchi, K. Matsuda, *Nano Lett.* **2013**, *13*, 5944–5948.
[72] Y. R. Shen, *Surface Properties Probed by Second-Harmonic and Sum-Frequency Generation* **n.d**.
[73] S. Yamaguchi, T. Tahara, *J. Phys. Chem. C* **2015**, *119*, 14815–14828.
[74] E. Collini, *Chem. Soc. Rev.* **2013**, *42*, 4932–4947.
[75] P. Hamm, M. Zanni, *Concepts and Methods of 2D Infrared Spectroscopy* **2011**.
[76] S. Mukamel, N. Y. Oxford, *PRINCIPLES OF NONLINEAR OPTICAL SPECTROSCOPY* **1995**.
[77] S. H. Aleithan, M. Y. Livshits, S. Khadka, J. J. Rack, M. E. Kordesch, E. Stinaff, *Phys. Rev. B* **2016**, *94*, DOI 10.1103/PhysRevB.94.035445.
[78] T. Goswami, R. Rani, K. S. Hazra, H. N. Ghosh, *J. Phys. Chem. Lett.* **2019**, 3057–3063.
[79] A. Singh, G. Moody, K. Tran, M. E. Scott, V. Overbeck, G. Berghäuser, J. Schaibley, E. J. Seifert, D. Pleskot, N. M. Gabor, J. Yan, D. G. Mandrus, M. Richter, E. Malic, X. Xu, X. Li, *Phys. Rev. B* **2016**, *93*, DOI 10.1103/PhysRevB.93.041401.
[80] F. Gao, Y. Gong, M. Titze, R. Almeida, P. M. Ajayan, H. Li, *Phys. Rev. B* **2016**, *94*, DOI 10.1103/PhysRevB.94.245413.
[81] D. Li, C. Trovatello, S. Dal Conte, M. Nuß, G. Soavi, G. Wang, A. C. Ferrari, G. Cerullo, T. Brixner, *Nat. Commun.* **2021**, *12*, DOI 10.1038/s41467-021-20895-0.
[82] L. Wibmer, S. Lages, T. Unruh, D. M. Guldi, *Adv. Mater.* **2018**, *30*, DOI 10.1002/adma.201706702.
[83] T. Godde, D. Schmidt, J. Schmutzler, M. Aßmann, J. Debus, F. Withers, E. M. Alexeev, O. Del Pozo-Zamudio, O. V. Skrypka, K. S. Novoselov, M. Bayer, A. I. Tartakovskii, *Phys. Rev. B* **2016**, *94*, DOI 10.1103/PhysRevB.94.165301.
[84] J. Pandey, A. Soni, *Appl. Surf. Sci.* **2019**, *463*, 52–57.
[85] T. Deilmann, K. S. Thygesen, *Nano Lett.* **2018**, *18*, 1460–1465.
[86] A. Chernikov, T. C. Berkelbach, H. M. Hill, A. Rigosi, Y. Li, O. B. Aslan, D. R. Reichman, M. S. Hybertsen, T. F. Heinz, *Phys. Rev. Lett.* **2014**, *113*, DOI 10.1103/PhysRevLett.113.076802.
[87] A. Singh, G. Moody, K. Tran, M. E. Scott, V. Overbeck, G. Berghäuser, J. Schaibley, E. J. Seifert, D. Pleskot, N. M. Gabor, J. Yan, D. G. Mandrus, M. Richter, E. Malic, X. Xu, X. Li, *Phys. Rev. B* **2016**, *93*, DOI 10.1103/PhysRevB.93.041401.
[88] R. Matsunaga, K. Matsuda, Y. Kanemitsu, *Phys. Rev. Lett.* **2011**, *106*, DOI 10.1103/PhysRevLett.106.037404.
[89] A. Ramasubramaniam, *Phys. Rev. B: Condens. Matter Mater. Phys.* **2012**, *86*, DOI 10.1103/PhysRevB.86.115409.
[90] G. Bastard, E. E. Mendez, L. L. Chang, L. Esaki, *Exciton Binding Energy in Quantum Wells* **n.d**.
[91] G. Finkelstein, V. Umansky, I. Bar-Joseph, V. Ciulin, S. Haacke, J.-D. Ganièe, B. Deveaud, *PHYSICAL REVIEW B 15 NOVEMBER 1998-I VOLUME* **n.d**.
[92] E. Vanelle, M. Paillard, X. Marie, T. Amand, P. Gilliot, D. Brinkmann, R. Lé, J. Cibert, S. Tatarenko, *Spin Coherence and Formation Dynamics of Charged Excitons in CdTeÕCd 1ÀxÀy Mg x Zn y Te Quantum Wells* **n.d**.
[93] D. Sanvitto, R. A. Hogg, A. J. Shields, M. Y. Simmons, D. A. Ritchie, M. Pepper, *Phys. Status Solidi B* **2001**, *227*, 297–306.
[94] J. S. Ross, S. Wu, H. Yu, N. J. Ghimire, A. M. Jones, G. Aivazian, J. Yan, D. G. Mandrus, D. Xiao, W. Yao, X. Xu, *Nat. Commun.* **2013**, *4*, DOI 10.1038/ncomms2498.
[95] T. Nishihara, Y. Yamada, M. Okano, Y. Kanemitsu, *Appl. Phys. Lett.* **2013**, *103*, DOI 10.1063/1.4813014.
[96] T. Koyama, S. Shimizu, Y. Miyata, H. Shinohara, A. Nakamura, *Phys. Rev. B: Condens. Matter Mater. Phys.* **2013**, *87*, DOI 10.1103/PhysRevB.87.165430.

Manuscript received: March 18, 2024
Accepted manuscript online: May 7, 2024
Version of record online: June 19, 2024